Sensors & Transducers, Vol. 155, Issue 8, August 2013, pp. 262-270

www.sensorsportal.com

Sensors & Transducers

http://www.sensorsportal.com

Improving the Lorentz Force Amplitude of an EMAT Using Stacked Coil Configuration

[1] Evans Ashigwuike, [1] Wamadeva Balachandran, [2] Sadiq Thomas, [1] Nadaraja Manivannan, [1] Ruth Mackay

[1] Centre for Electronic System Research, Brunel University Uxbridge, Middlesex, UB83PH

[2] Herriot Watt University, School of Built Engineering, Institute for Infrastructure & Environment, Edinburgh, E14 4AS, UK

Tel.: +44(0)1895265774, fax: +44(0)1895258728

E-mail: evans.ashigwuike@brunel.ac.uk, s.thomas@hw.ac.uk

Received: 16 May 2013 /Accepted: 12 August 2013 /Published:20 August 2013

Abstract: This research presents a study of a novel method of improving the Lorentz force amplitude of a planer spiral coil EMAT configuration by stacking the coils. A 2D axisymmetric Finite Element Model was developed to study and compare the density of the Lorentz Force (LF) generated at the skin depth by the Stacked Spiral-EMAT (SS-EMAT) configuration on cs70 grades of pipe steel materials. The response of the novel EMAT configuration to variation of parameters such as the static magnetic field, internal diameter, excitation frequency, lift-off, coil stacking, the thickness of the insulation layer and number of cycles per tone burst were also investigated to ascertain the viability of the Stacked Spiral-EMAT. The results obtained showed that there is a significant improvement in the density of Lorentz Force generated by the novel EMAT when stacked. Hence a new EMAT configuration is proposed to enhance the performance of radially polarised bulk wave EMATs. *Copyright © 2013 IFSA.*

Keywords: Lorentz force, Electromagnetic acoustic transducer, Eddy current.

1. Introduction

Electromagnetic Acoustic Transducers (EMATs) can generate and detect ultrasonic wave without making contact with the test material. This feature makes it an attractive option in contactless measurement such as when carrying out inspection in high temperature environment or taking measurement in a moving object [1-3]. EMATs have also found usefulness in many non-destructive evaluation applications, such as the determination of physical parameters of conducting materials, flaw characterization, dimension and thickness measurement. EMATs consist of coils and permanent or electromagnet located in proximity to the surface of the material. The coils are excited with a high frequency tone burst pulse, this creates a dynamic magnetic field which further induces a high frequency eddy current on the conducting material [1, 4]. The interaction of the eddy current and the static magnetic field (bias field) gives rise to mechanical strain and hence produces ultrasonic waves on the material [1, 4, 5]. The outcome of researches during the last couple of years on the performance of EMAT on conducting materials (ferro-magnetic and non-ferromagnetic material) have been reported [6-9]. The reports have established that EMAT has low transduction efficiency which gives rise to reduced signal to noise ratio (SNR). In other to increase the signal to noise

ratio of EMAT, several attempts have been made to improve the performance of EMATs 10-18].

In [19] it was established that LF mechanism is the dominant transduction mechanism for normal biased EMATs configuration on ferro-magnetic materials. Table 1 shows the measured electromagnetic properties of the grade of steel (pipe steel) used in this study.

The research paper presents a 2 D axisymmetric finite element model of a Stacked spiral EMAT coil configuration and a novel stacked spiral EMAT (SS-EMAT) coil configuration to optimize the generation of ultrasonic wave on steel material based in LF mechanism. This is achieved by improving the strength of LF generated by the EMAT system. The SS-EMAT model is an improvement on the conventional planner circular spiral coil configurations.

Fig. 2: 2D Representation of SS-EMAT showing Eddy current, static field and effective Lorentz force; (a) single coil layer over pipe steel specimen; (b) stacked (two) coil layer over pipe steel specimen; (c) proposed stacked (three) coil layer over pipe steel specimen. All drawings are to scale.

Table 1. Measured Electromagnetic properties of CS70 grade of pipe steel material [6].

Material designation	Relative permeability μ_r	Electrical Conductivity (S/m)
CS70	59	3.77×10^6

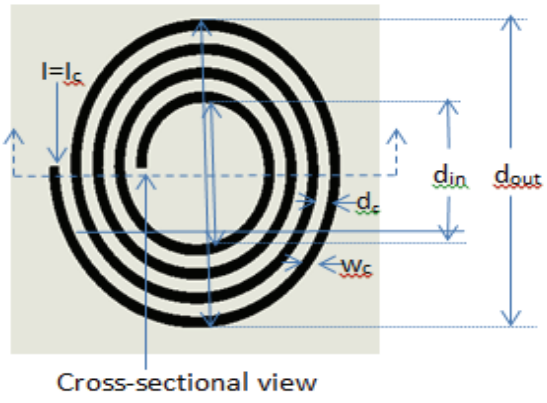

Fig. 1. The structural diagram of a circular planner spiral coil.

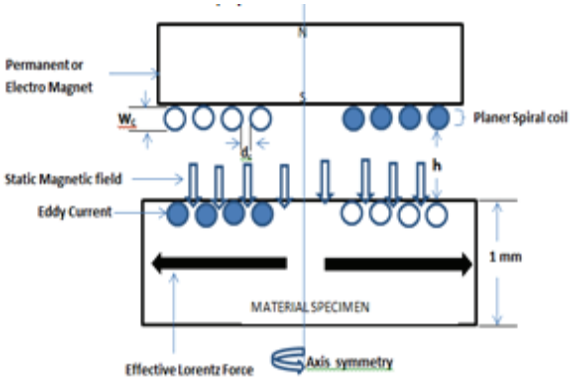

(a)

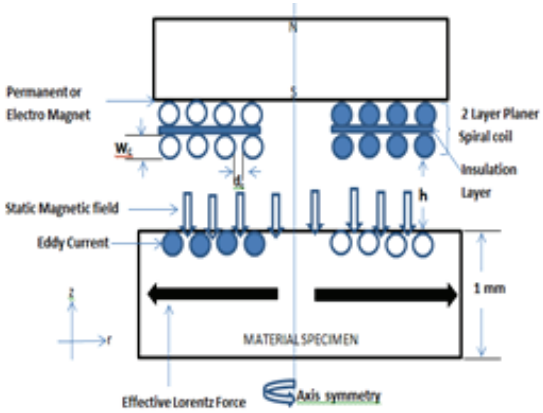

(b)

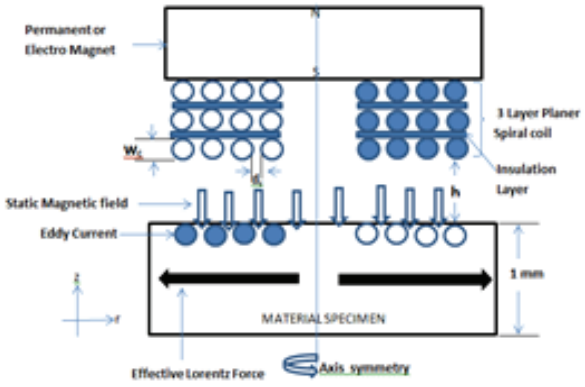

(c)

Fig. 2. 2D Representation of SS-EMAT showing Eddy current, static field and effective Lorentz force.

2. Theory

This analysis is based on the fact that in normal bias EMAT structure, LF has been proven to be the dominant transduction mechanism for both Ferro-magnetic and non ferro-magnetic materials [20].

Lorentz force is generated as a result of the interaction between the magnetic flux density and the eddy current density $\vec{J}_E$ induced by a coil excited with a sinusoidal current. The sinusoidal excitation current generate dynamic flux density $\vec{B}_d$ as well as Eddy current $\vec{J}_E$ in the steel plate. The Eddy current experiences a Lorentz force under the interaction of the dynamic magnetic field from the excitation current and the static magnetic field $\vec{B}_s$ from the permanent or electromagnet. The LF causes the vibration of the atomic structure of the material, which then leads to the generation of acoustic wave inside the conducting material. Generally, the direction and strength of the LF is governed by the following vector equations [21].

$$\nabla\times\vec{H}_d=\vec{J}_E, \tag{1}$$

$$\vec{B}_d=\mu_r\vec{H}_d, \tag{2}$$

$$\nabla\times\vec{E}_E=-\partial\vec{B}_d/\partial t, \tag{3}$$

$$\vec{J}_E=\sigma\vec{E}_E, \tag{4}$$

$$\vec{f}_d=\vec{J}_E\times\vec{B}_d, \tag{5}$$

$$\vec{f}_s=\vec{J}_E\times\vec{B}_s, \tag{6}$$

$$\vec{f}_L=\vec{f}_d+\vec{f}_s, \tag{7}$$

$$\vec{F}_L=\int\int\int_v\vec{f}_L\,dV, \tag{8}$$

where μ_r and σ, are the relative permeability and conductivity of CS70 grade of pipe steel; $\vec{E}_E$, $\vec{H}_d$ are the electric field intensity and dynamic magnetic intensity respectively; $\vec{f}_d$ and $\vec{f}_s$ are the Lorentz force densities due to the dynamic and static magnetic field respectively; $\vec{f}_L$ is the composite Lorentz force densities of $\vec{f}_d$ and $\vec{f}_s$; and $\vec{F}_L$ is the Lorentz force on a given volume, where ρ is mass volume density and τ and μ are the Lamé constants.

3. Finite Element Modelling

The structure of the EMAT considered in this research is shown in Fig. 2. In Fig. 2 (a), the structure consist of a rectangular meander-line coil, Fig. 2 (b) consist of a planer spiral coil while Fig. 2 (c) and Fig. 2 (d) consist of the novel single and double layer SS-EMAT coil respectively. Each structure consists of identical cross-sectional area of thickness t_c, width w_c, a permanent magnet and pipe steel specimen of 1mm thick. The lift off distance between the rectangular coils and the steel specimen is "h" and the distance between each coil turn is denoted as "d". In Fig. 2 (b) and Fig. 2 (c), the internal diameter of the coil is denoted as "d_{in}".

A 2D axis symmetrical finite element model was established using a commercial software called ComsolMultiphysics®, as shown in Fig. 5.

The coil was excited with a transient current [11]:

$$i_k(t)=\begin{cases}(-1)^k I_0\left[1-\cos\left(\frac{w_0 t}{n}\right)\right]\cos(w_0 t), \\ \quad for\ 0\le t\le(2n\pi)/w_0 \\ 0, \quad for \quad t\ge(2n\pi)/w_0\end{cases} \tag{9}$$

where I_0, w_0 and n are the amplitude of the current, the angular centre frequency and the number of cycles respectively.

$$w_0=2\pi f_0 \tag{10}$$

Fig. 3 shows the time history of external current density of the SS-EMAT at 30 A.

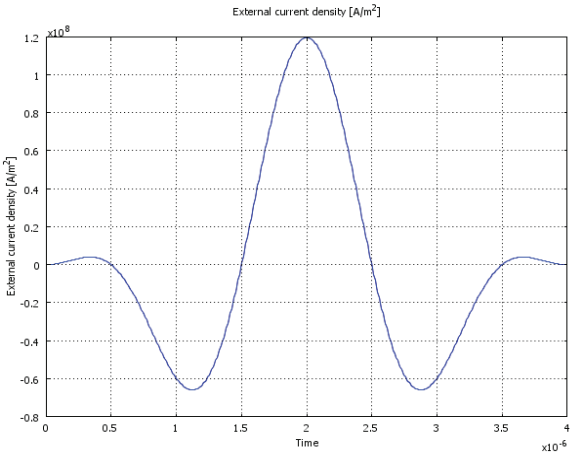

Fig. 3. Time history of the External current density of three layer SS-EMAT (I_0=30 A).

3.1. Modelling of Single Layer PS-EMAT

The parameters used for the simulation of the 1 layer SP-EMAT in Fig. 2 (a) are: f_0=500 kHz, n=2, I_0=30 A, B_0=1.2 T, W_c=0.8 mm, d_{in}=5 mm, d_c=0.1 mm and h=0.5 mm.

3.2. Modelling of Proposed Stacked SP-EMAT

The simulation was carried out using the same coil parameters as in 3.2 above but with adjustment in the number of layers of the coil to two in Fig. 2 (b) and three in Fig. 2 (c). An insulation layer thickness (t_{in}) of 0.1 mm was also included in the model. The insulation layer was modelled as a composite polymer (Z1258 anti rust silicone baffle paint) with performance index as presented in Table 2 [23].

Table 2. Performance index of Z1258 anti rust silicone baffle paint [23].

No.	Index name	Unit	Index
1.	Appearance		The film becomes bright after drying
2.	Viscosity	S	≥40
3.	Content of solid (10 g paint, (23±2^0 C/h)	%	55±5
4.	Drying time under room temperature	H	≤24
5.	Dielectric strength	MV/m	≥30
6.	Volume resistivity	Ω-m	≥ 1×10^8
7.	Fineness (scrapper fineness meter)	μm	≤45
8.	Adhesion coil	grade	1~2

3.3. Finite Element Mesh

The finite element model was obtained by discretising the physical model in to numerous second order quadratic triangular elements consisting of 6555 elements. The mesh element were refined at about 0.2 mm around the skin depth surface of the steel material and around the excitation coil with minimum element quality of 0.04897. This refinement of the model significantly improves its accuracy. Though the number of elements as wells as the solution time was greatly increased. This is achieved by continuously comparing the calculated result at different degree of refinement until when the result hardly changes with refinement as shown in Fig. 4.

To obtain a more precise result, the time steps, relative tolerance and the absolute tolerance of then finite element model were adjusted.

4. Simulation and Analisis

Applying the external source current in equation (9) and the static magnetic field in the finite element model, equation (8) is solved to obtain the Lorentz force density in the steel as shown in Fig. 5. Also to obtain an accurate record of the time variation of the Lorentz force from the simulation, the 2D axis symmetrical model was revolved about its axis, and a 3D surface plot was obtained. A line extrusion plot of the Lorentz force obtained at the skin depth of the steel material for both the single layer and multi-layer SS-EMAT as shown in Fig. 6, Fig. 7 and Fig. 8.

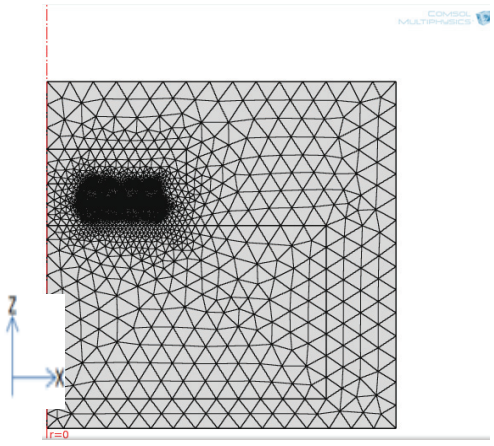

Fig. 4. Finite element mesh of the model used.

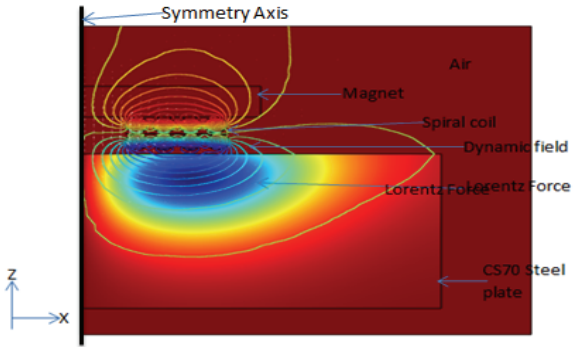

Fig. 5. Axi-symmetrical FE model of a stacked three layer SS-EMAT.

4.1. Influense of Coil Stacking on the Lorentz Force Density

As shown in equation (5), the dynamic magnetic field generated by the EMATs coil is a very important factor that influence the performance of EMATs in general. To improve the strength of the dynamic Lorentz force, the coils were stacked in layers and connected in series. The stacked coils were excited with a tone burst sinusoidal pulse as in equation (9). Fig. 6, Fig. 7 and Fig. 8 shows a 3D surface plot of a single, two and three layers SS-EMAT. The values of the density of LF were obtained by measuring the peak to peak value of the surface plot. This procedure was repeated to obtain the LF density for various number of coils in a stack as shown in Fig. 9. The values of the LF density obtained was 3.1×10^8 N/m^3, 1.9×10^9 N/m^3 and 3.5×10^9 N/m^3 for the single layer, two layers and three layers respectively.

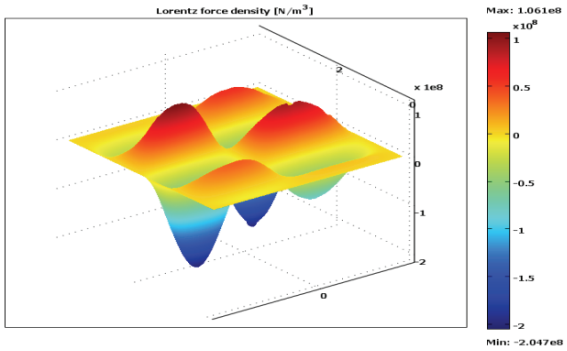

Fig. 6. 3D line extrusion surface plot of the Lorentz force generated by a single layer PS-EMAT.

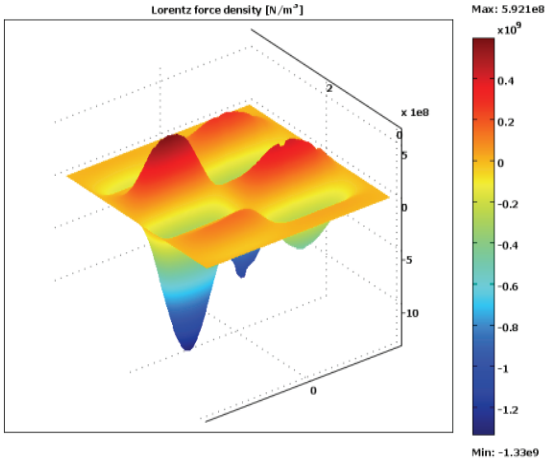

Fig. 7. 3D line extrusion surface plot of the Lorentz force generated by a Two layer SS-EMAT.

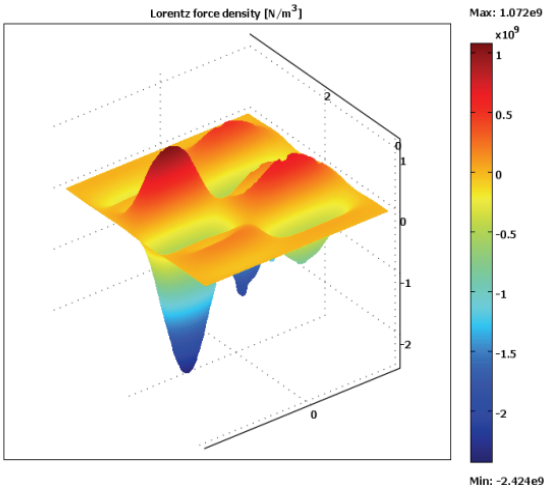

Fig. 8. 3D cross section linear extrusion surface plot of the Lorentz force generated by a Three layer SS-EMAT.

It was observed that the density of the LF in the materials increases exponentially with the increase in the number of coils in the stack/layers and saturates when the number of coil increases beyond eight coils per stack. Any further increment in the number of coil beyond this point yielded no significant increase in the Lorentz force density. This is expected since an increase in the number of coils in a stack, translates to an increase in the total dynamic magnetic flux. Beyond the Eighth coil, the distance between the coil and the specimen (lift off) will be enough as to obscure the effect of the additional coil, hence no significant increment was observed beyond nine coil per stack. Also, it worthy to note that in practice, an increment in the number of coil per stack does not lead to excessive heating due to the fact that the duration of the excitation current is typically at micro-second level [21]. Therefore, the SS-EMAT configuration performs optimally when the number of coil in a stack does not exceed 8.

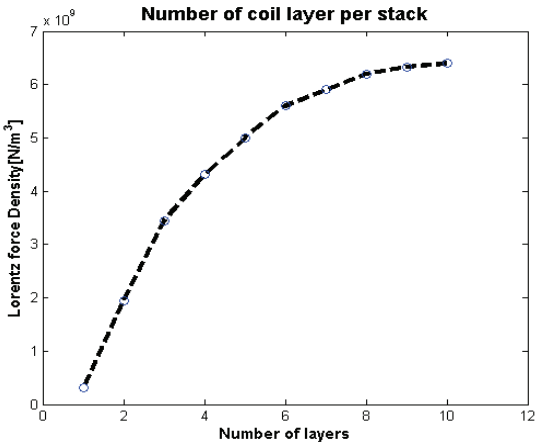

Fig. 9. LF strength under different number of coil layers.

4.2. Influence of Lift-off Distance on the Lorentz Force Density

The performance of the single, two and three layer stacked SS-EMAT configuration on CS70 grade of pipe steel was investigated, by varying the lift-off distance from 0.5 mm to 8 mm above the surface of the steel specimen. The measurement of LF density was taken within the skin depth (at about 0.1 mm below the surface) of the material specimen at the second turn of the coil. The results shown in Fig. 10 indicates that the LF density decreases exponentially with the lift-off distance with the three layer SS-EMAT configuration having the best lift off characteristics, followed by the two Layered configuration. This phenomenon also confirms the correlation between the coil layers, the dynamic magnetic field, and the LF and is in good agreement with findings of [22]. The results also indicates that for single and two layers SS-EMAT configuration, any increase beyond 4.0 mm and 4.5 mm respectively of lift off, the LF generated in the specimen is almost zero. While for three layer SS-EMAT, the same effect was observed beyond 5.5 mm of lift-off. This further indicates that there is a significant improvement in the lift off distance from 1 mm-3 mm obtained in most commercial EMAT [1] to 1 mm-5 mm.

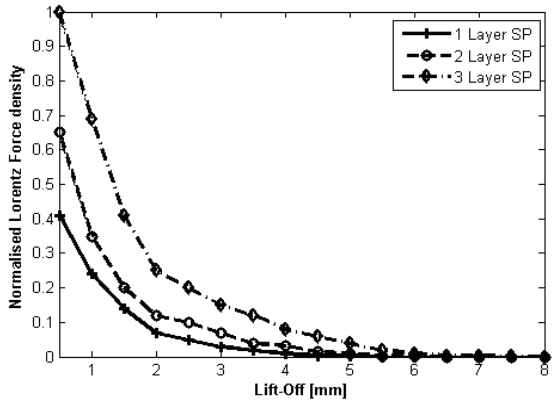

Fig. 10. Variation of Lift off distance with the number of coils per stack, on CS70 grade of pipe steel.

4.3. Influense of Coil Internal Diameter (d_{in}) on the Lorentz Force Density

Fig. 11 shows a correlation between the internal diameter of the three layer SS-EMAT coil and LF density generated on the surface of the pipe steel specimen. As the internal diameter is increased the LF also increases up to about 14 mm, at this point any further increment has no noticeable effect on the LF density. This phenomenon is because as the internal diameter is increased, the interaction between opposing dynamic magnetic field in the coil is reduced. This continues up to a point where there will be little or no effect of the opposing field. Therefore, for optimal performance of this stacked PS-EMAT configuration, the internal diameter must be greater than 14 mm.

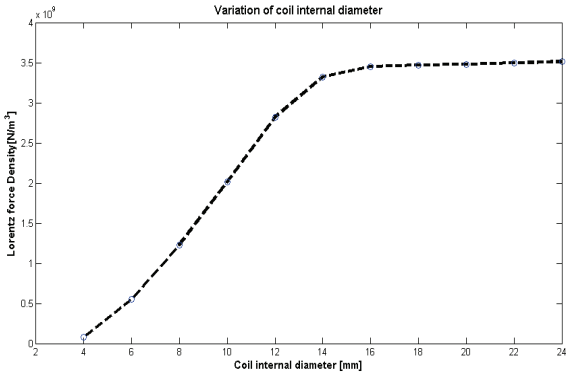

Fig. 11. LF strength under different internal diameter of SS-EMAT.

4.4. Effect of Variation of Static Flux Density (B_0) on the Lorentz Force Density

The static flux density is another important factor that affects the performance of EMATs, hence the need to investigate its effect on the LF generated by the three layer SS-EMAT, on the material specimen. Fig. 12 shows the result of the simulation obtained by varying the static magnetic field from 0.5 T to 2.0 T. The result shows that by increasing the static magnetic flux, the LF generated in the material specimen also increases and vice versa. At 0.5 T, the peak to peak value of the LF is 3.0×10^9 N/m^3 while the value of 2.0 T produced the highest LF of 4.7×10^9 N/m^3. The time variation of the LF was observed not be affected by the variation of the magnetic flux density. The result is in good agreement with published work of [9].

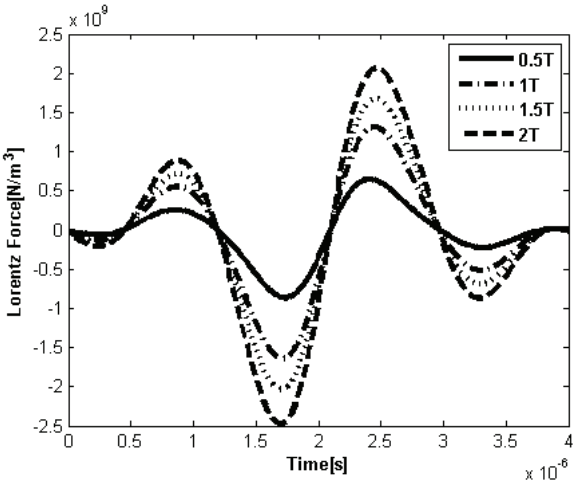

Fig. 12. Time variation of static flux density B_0 from (0.5 T to 2.0 T).

4.5. Effect of Variation of Insulation Layer Thickness (t_{in}) on the Lorentz Force Density

As observed in section 3.4, stacking coils in layers improves the performance of the SS-EMAT. To prevent short circuiting and binding the coils tightly together, they are coated with insulation material. The insulation material used for this simulation was Z1258 Anti-rust silicone baffle paint and has the following properties [23]:

(i) Good heat resistance
(ii) Firm adhesion
(iii) Short drying period
(iv) High dielectric strength of 30×10^6 V/m.

Fig. 13 shows the result of the simulation obtained by varying the insulation thickness from 0.1 mm to 2.5 mm. The result implies that, the LF strength decreases exponentially with increasing insulation thickness. The highest value of LF strength of 1.95×10^9 N/m^3 was obtained at insulation thickness of 0.1 mm while the least value of 1.1×10^9 N/m^3 was obtained at a thickness of 2.5 mm. Therefore, for optimal performance of the KT coil, the insulation thickness must not exceed 1 mm. The performance index of Z1258 anti rust silicone baffle paint is given in Table 2.

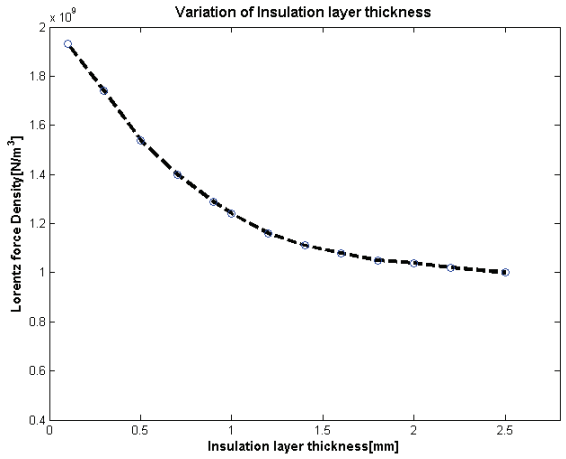

Fig. 13. Variation of insulation layer thickness from (0.1 mm to 10 mm).

4.6. Effect of Variation of Excitation Period on the Lorentz Force Density

It has been shown in [22] that the period number of a tone burst signal, determines the quantity of energy transferred from the power source to the coil, which has a direct effect on the LF strength and mechanical energy generated. This implies that more period number gives rise to more excitation energy. In the previous results (Fig. 5 to Fig. 13) the SS-EMATs were excited with a 2 period tone burst signal. To understand the effect of variation of the number of periods on the SS- EMAT under a given excitation current amplitude and frequency of 30 A and 500 kHz respectively, the number of period of the tone burst signal was varied in the following sequence (2 to 12) with all other parameters remaining unchanged. The result shows that an increase in the period, leads to an increase in the width of the LF wave packet (Fig. 14 (a) and Fig. 14 (b)). Analysing the result further, a linear relationship was established between the LF strength and the variation in the number of periods of the tone burst signal, see Fig. 14 (c).

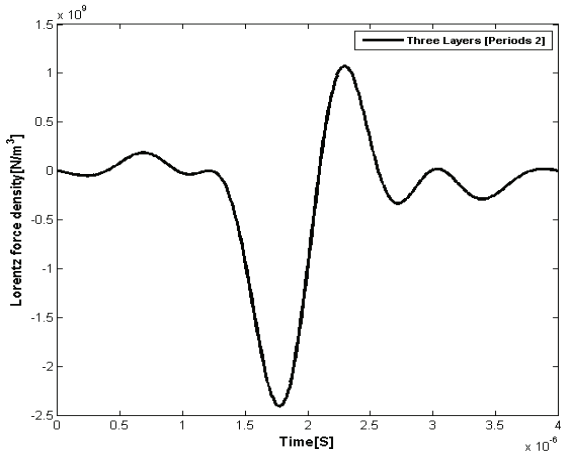

Fig. 14 (a). Lorentz force density for three layer SS-EMAT under different period number: 2 periods.

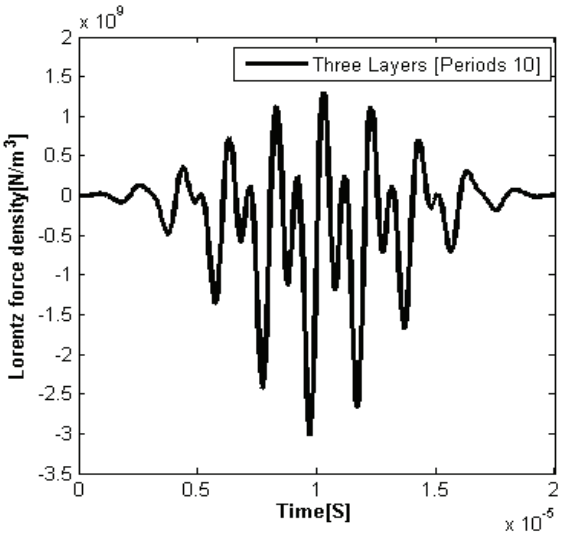

Fig. 14 (b). Lorentz force density for three layer SS-EMAT under different period number: 10 periods.

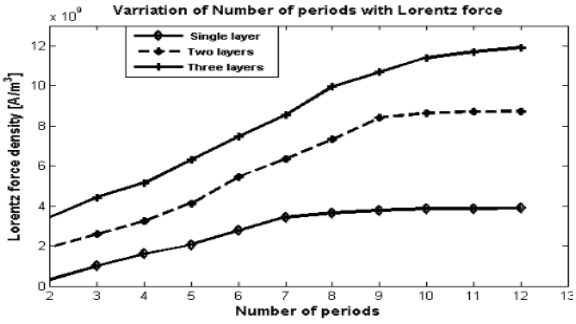

Fig. 14 (c). Variation of Lorentz force density with the number of periods from (2 to 12).

4.7. Effect of Variation of Excitation Frequency on the Density of Lorentz Force

To investigate the effect of variation of excitation frequency on the density of the LF generated by the proposed Three layer SS-EMAT, the static field and the excitation current were maintained at 0.7 T and 30 A respectively.

The excitation frequency was varied from 500 kHz to 8 MHz, and the corresponding change in LF generated in the material specimen was calculated. Fig. 15, shows that the LF density increases as the excitation frequency varies from 0.5 MHz and reached a peak value a at 4.5 MHz, thereafter it starts decreasing with a more pronounced effect seen in the three layer PS-EMAT. This implies that any increase in frequency beyond 4.5 MHz has a negative effect on the density of the LF generated in the material specimen. Hence for optimal performance of this EMAT, the right excitation frequency between 2.5 and 5 MHz should not be exceeded. This result is in good agreement with work published by [18].

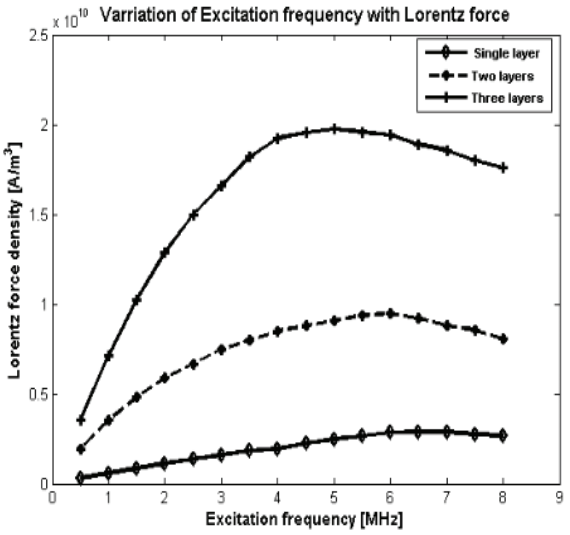

Fig. 15. Variation of LF density with excitation frequency.

5. Conclusion

In this research, a novel stacked PS-EMA transducer was presented and studied. Also, a 2D axis symmetrical finite element model in the time domain was successfully developed and implemented, we have used the model to study the effect of some parameters on the performance of a novel SS-EMAT configuration. The study carried out in the first stage includes calculating and comparing the LF density generated by the three SS-EMAT configuration (single, two and three layers) on CS70 grade of pipe steel material. The second stage of the study investigated the effect of variation of some EMAT parameters (such as coil internal diameter, lift off, coil width, excitation frequency, coil stacking, insulation layer thickness and excitation period) on the LF generated by the SS-EMAT configuration. The numerical results were in good agreement with previous work done by other researchers. According to the study, the proposed SS-EMAT is effective in improving the Lorentz force density, which is a very good parameter required for non destructive testing of steel materials. This is so because an increase in the Lorentz force density leads to a corresponding increase in the strength of the acoustic signal generated on the material specimen.

The result also shows that close attention should be paid to the these EMAT parameters in other to obtained accurate measurement using the SS-EMAT configuration.

References

[1]. M. Hirao and H. Ogi, EMATs for Science and Industry: Noncontacting Ultrasonic Measurements, *Springer*, 2003.

[2]. B. Maxfield and C. Fortunko, The design and use of Electromagnetic Acoustic Wave Transducers (EMATs), *Mater. Eval.,* Vol. 41, 1983, pp. 1399-1408.

[3]. E. Dobbs, Electromagnetic generation of ultrasonic waves, *Physical Acoustics,* Vol. 10, 1973, pp. 127-189.

[4]. T. Kundu, Ultrasonic nondestructive evaluation: engineering and biological material characterization, *CRC Press,* 2003.

[5]. G. Alers, A history of EMATs, in *Proceedings of the AIP Conference,* 2008, p. 801.

[6]. R. Ribichini, F. Cegla, P. Nagy and P. Cawley, Experimental and numerical evaluation of electromagnetic acoustic transducer performance on steel materials, *NDT E Int.,* Vol. 45, 2012, pp. 32-38.

[7]. R. Jafari-Shapoorabadi, A. Konrad and A. Sinclair, The governing electrodynamic equations of electromagnetic acoustic transducers, *J. Appl. Phys.,* Vol. 97, 2005, pp. 10E102-10E102-3.

[8]. R. Dhayalan, V. Satya Narayana Murthy, C. Krishnamurthy and K. Balasubramaniam, Improving the signal amplitude of meandering coil EMATs by using ribbon soft magnetic flux concentrators (MFC), *Ultrasonics,* Vol. 51, 2011, pp. 675-682.

[9]. S. Thomas, S. Obayya, R. Taneja and W. Balachandran, A Coupled Electromagnetic and Mechanical Analysis of Electromagnetic Acoustic Transducers, *International Journal for Computational Methods in Engineering Science and Mechanics,* Vol. 10, 2009, pp. 124-133.

[10]. H. Ogi, Field dependence of coupling efficiency between electromagnetic field and ultrasonic bulk waves, *J. Appl. Phys.,* Vol. 82, 1997, pp. 3940-3949.

[11]. R. Jafari-Shapoorabadi, A. Konrad and A. Sinclair, Improved finite element method for EMAT analysis and design, *IEEE Transactions on Magnetics,* Vol. 37, 2001, pp. 2821-2823.

[12]. R. Ludwig, Z. You and R. Palanisamy, Numerical simulations of an electromagnetic acoustic transducer-receiver system for NDT applications, *IEEE Transactions on Magnetics,* Vol. 29, 1993, pp. 2081-2089.

[13]. M. Kaltenbacher, K. Ettinger, R. Lerch and B. Tittmann, Finite element analysis of coupled electromagnetic acoustic systems, *IEEE Transactions on Magnetics,* Vol. 35, 1999, pp. 1610-1613.

[14]. R. B. Thompson, A model for the electromagnetic generation of ultrasonic guided waves in ferromagnetic metal polycrystals, *IEEE Transactions on Sonics and Ultrasonics,* Vol. 25, 1978, pp. 7-15.

[15]. R. S. Edwards, X. Jian, Y. Fan and S. Dixon, Signal enhancement of the in-plane and out-of-plane Rayleigh wave components, *Appl. Phys. Lett.,* Vol. 87, 2005, pp. 194104-194104-3.

[16]. X. Jian, S. Dixon and R. S. Edwards, Ultrasonic generation and optimization for EMAT, in *Proceedings of the AIP Conference,* 2005, p. 1041.

[17]. X. Jian and S. Dixon, Enhancement of EMAT and eddy current using a ferrite back-plate, *Sensors and Actuators A: Physical,* Vol. 136, 5/1, 2007, pp. 132-136.

[18]. M. Kaltenbacher, R. Lerch, H. Landes, K. Ettinger and B. Tittmann, Computer optimization of electromagnetic acoustic transducers, in *Proceedings of the IEEE Ultrasonics Symposium,* 1998, pp. 1029-1034.

[19]. Ribichini, F. Cegla, P. B. Nagy and P. Cawley, Quantitative modeling of the transduction of electromagnetic acoustic transducers operating on ferromagnetic media, *IEEE Transactions on*

Ultrasonics, Ferroelectrics and Frequency Control, Vol. 57, 2010, pp. 2808-2817.
[20]. R. Ribichini, P. Nagy and H. Ogi, The impact of magnetostriction on the transduction of normal bias field EMATs, *NDT E Int.,* 2012.
[21]. S. Wang, L. Kang, Z. Li, G. Zhai and L. Zhang, 3-D modeling and analysis of meander-line-coil surface wave EMATs, *Mechatronics,* Vol. 22, 9, 2012, pp. 653-660.
[22]. Hao Kuang Sheng, Huang Song Ling, Zhao Wei and Wang Shen, Multi-belt coil longitudinal guided wave magnetostrictive transducer for ferromagnetic pipes testing, *Science China Technological Science*, Vol. 54, No. 2, February 2011.
[23]. Transformer coil coating - Technical manual, Zhuzhou Insulation Material, Co. Ltd.